From plasmon-induced luminescence enhancement in gold nanorods to plasmon-induced luminescence turn-off: a way to control reshaping

Céline Molinaro, Sylvie Marguet, Ludovic Douillard, Fabrice Charra, Céline Debuisschert

From plasmon-induced luminescence enhancement in gold nanorods to plasmon-induced luminescence turn-off: a way to control reshaping

Céline Molinaro, Sylvie Marguet, Ludovic Douillard, Fabrice Charra and Céline Fiorini-Debuisschert

The two-photon luminescence (TPL) turn-off in small single gold nanorods (GNR) exposed at increased resonant femtosecond laser excitation (800 nm wavelength, pulse energy density varying from 125 μJ.cm^{-2} to 2.5 mJ.cm^{-2}) is investigated. The origin is shown to be a photo-induced decrease of the rod aspect ratio. Such aspect ratio reduction could reasonably be assigned to gold atom diffusion away from the rod tips, where hot spots are localized. The two-photon luminescence signal can be recovered after a blue-shift of the incident excitation wavelength. In case the excitation wavelength is not changed, there results an out of resonance excitation of the rods and thus a reduced absorption, acting as a feedback to stabilize the GNR shape and size. A theoretical analysis is presented evidencing limited thermal effects in the femtosecond regime for small nanoparticles, in good agreement with complementary topographic characterizations using scanning electron microscopy (SEM) and atomic force microscopy (AFM). We show finally that TPL reveals itself as a highly sensitive tool to follow tiny changes resulting from the photo-induced reshaping of GNRs.

A Introduction

Plasmonic luminescence has been the subject of intense work and debates over the last years.[1–6] Although bulk gold is known to present a very low luminescence quantum yield,[7] gold nanostructures exhibit a huge nonlinear luminescence with a high influence of the particle morphology (shape and size).[8] More particularly, gold nanorods display one of the highest emission signal with a two-photon brightness a few million times higher than the two-photon brightness of a classical organic fluorophore such as fluorescein.[9]

This large two-photon luminescence of colloidal gold nanorods can be shown to be the result of a so-called "double antenna effect" in direct connection with the two different GNR localized surface plasmon resonances, λ_{TR} around 520-540 nm for the transverse resonance (TR) and λ_{LR} above 750 nm for the longitudinal resonance (LR), the latter being directly dependent on the GNR aspect ratio.[10] Excitation of one GNR at its longitudinal plasmon frequency ($\lambda_{exc} \approx \lambda_{LR}$) first leads to an increased absorption and thus an increased production of electron-hole pairs which subsequently recombine radiatively through the transverse plasmon band ($\lambda_{em} \approx \lambda_{TR}$), i.e. with an enhanced emission at the transverse plasmon band.[9]

At larger time scales, electron-phonon interactions offer another decay mechanism for hot electrons with potential applications in nanomedicine, phototherapy[11–13] or in material science for laser writing and patterning.[14] Depending on the incident power and pulse duration,[15] different types of plasmon-induced photothermal effects in nanorods were already observed such as fragmentation,[16] deformation into a nanosphere or reduction of the aspect ratio.[17] In water nanocavitation processes were evidenced under specific laser excitation.[18,19] Most previous studies have however been performed at the ensemble level,[18,20–22] detailed single particles studies being more scarce.[23,24] Reported experiments were also performed with a relatively high pulse energy density, i.e. higher [20,25,26] than few mJ.cm^{-2} with particles most often reaching their melting temperature.

In the study presented here, we consider the case of much lower energy densities working with single GNRs (10 nm diameter (Φ) , 40 nm length (l)) immobilized onto Indium Tin Oxide (ITO) coated glass substrates. We evidence photo-induced changes in these nanorods for incident energy densities as low as 125 μJ.cm^{-2}. The illumination of single GNRs at such energy density is more particularly observed to induce a huge drop in their TPL intensity. The photo-induced morphological change of a set of more than 10 single GNRs was studied in detail, correlating complete polarization resolved TPL characterizations with AFM and SEM complementary analyses. We show that TPL constitutes a very sensitive tool enabling to detect variation of plasmon resonances smaller than ten nanometers in wavelength, corresponding to tiny

morphological changes that happen to be difficult to identify using common direct imaging methods such as AFM or SEM. Finally, a theoretical analysis is presented evidencing limited thermal effects due to a fast outward heat release process intrinsic to the small objects considered here, and a complete temperature release between two successive laser pulses. This explains the absence of any melting of the rods.

B Methods

B-1 Sample preparation

GNRs (Φ = 10 nm, l = 40 nm) were synthesized using a colloidal seed-mediated procedure.[27,28] The extinction spectrum of these GNRs reveals two different plasmon resonances: a transverse resonance around 520 nm and a longitudinal one around 800 nm as expected from their aspect ratio (AR) of c.a. 4. These GNRs present a CTAB (Cetyl TrimethylAmmonium Bromide) capping layer which is positively charged. The positive charge of the CTAB surfactant can be taken into profit to immobilize the GNR using electrostatic interactions. For this, ITO coated substrates are first treated using UV-Ozone in order to produce negatively charged hydroxyl groups at the ITO surface, a droplet of GNRs in solution being consecutively left to dry. Nonspecifically coupled GNRs are then eliminated through careful rinsing with ethanol. In the case of glass slides, this electrostatic coupling cannot be produced and the GNRs happen to be less anchored, making AFM characterization more difficult but still possible. Thanks to specific landmarks fabricated on the substrates, each considered GNR can be precisely localized and the same single objects can successively be analyzed using TPL, SEM and AFM throughout the process (before and after high power excitation of each GNR).

B-2 Experimental set-up

The two-photon luminescence of single colloidal gold nanorods (Φ = 10 nm, l = 40 nm) was characterized using a channel plate multiplier (CPM) working in the photon counting mode (Perkin Elmer MP-993-CL). A specific set-up was developed in order to correlate the TPL properties of single GNRs with their geometry, orientation and environment. As displayed in Fig. 1, each GNR could simultaneously be characterized using two probes that need first to be aligned: (1) an AFM tip (ACTA Probes, AppNano) for the characterization in topography (NanoWizard III, JPK), and (2) a focused laser spot (microscope objective NA = 1.3 leading to a beam waist w = 400 nm) coupled to the sample through an inverted optical configuration, for the two-photon excitation of the nanorods. The AFM tip was shown to have no influence on the GNR TPL properties.

The laser (Tsunami, Spectra Physics, 100 fs pulses, 80 MHz – 740 nm < λ < 950 nm) was linearly polarized (a Babinet-Soleil compensator, positioned before the dichroic mirror 2, was used to compensate any depolarization effects in the optical path to the sample). Laser polarization together with average power could be controlled using sets of half-wave plates and polarizers. The same objective was used for excitation and collection of the GNR luminescence. In order to avoid any unwanted changes of the rods during characterization, TPL measurements were performed at reduced power (energy densities around F = 45 µJ.cm^{-2}). The AFM tip was retracted to prevent any damage when illuminating the GNR at high power (F > 100 µJ.cm^{-2}).

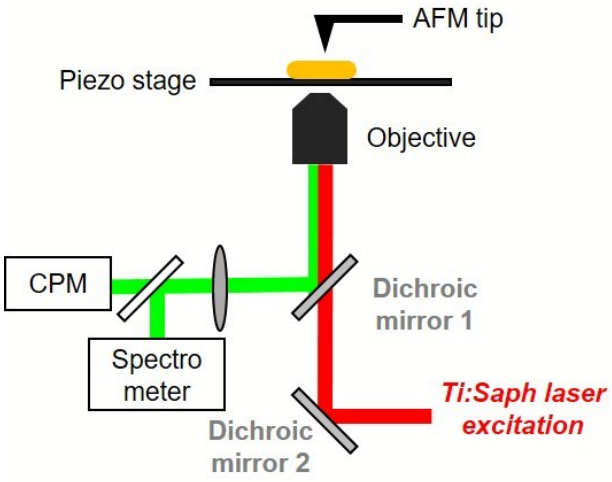

Fig. 1 Combined TPL and AFM microscopy set-up involving an inverted microscope (Olympus IX71) coupled to a cantilever type AFM platform (NanoWizard III, JPK) and associated to a femtosecond laser excitation. After alignment of the AFM tip with the focussed laser spot, the sample is raster scanned enabling simultaneous topography (tapping mode) and TPL recording. Excitation is performed through a dichroic mirror (SemRock FF750-SDi02-25x36) and an oil immersion 100x microscope objective. The emitted TPL is collected through the same microscope objective and separated from the incident light by another dichroic mirror (SemRock FF735-Di670-25x36). The signal is then sent either to a channel plate multiplier working in the photon counting mode (Perkin Elmer MP-993-CL) or to a spectrometer coupled to a CCD camera (Andor DU401-BR-DD) for detailed study of the emission spectra.

C Results and discussion

After deposition, the GNRs were investigated through correlated TPL and topography measurements (Fig. 2A and 2C). TPL spots of varying intensity were recorded depending on the relative orientation of the rods, with almost no observed TPL in the case of rods perpendicular to the excitation polarization direction. Indeed the GNR TPL is known to be highly dependent on the resonant excitation of their longitudinal plasmon resonance.[9] The orientation of each GNR was verified by taking SEM image of the same areas (Fig. S1). One GNR (blue circled in Fig. 2) was then chosen for a high resonant power laser exposure, which will be further referred as an "over-illumination" (λ = 800 nm, incident polarization along the long axis of the GNR, F = 125 µJ.cm^{-2}). Characterization of the same sample area was performed again at a reduced power using the same previously detailed procedure. As shown in Fig. 2A and 2B, the high power laser illumination was seen to lead to a drastic reduction of the TPL intensity by about an order of magnitude, with an apparent change in the GNR topography. This behavior was characteristic of all considered "over-illuminated" GNRs.

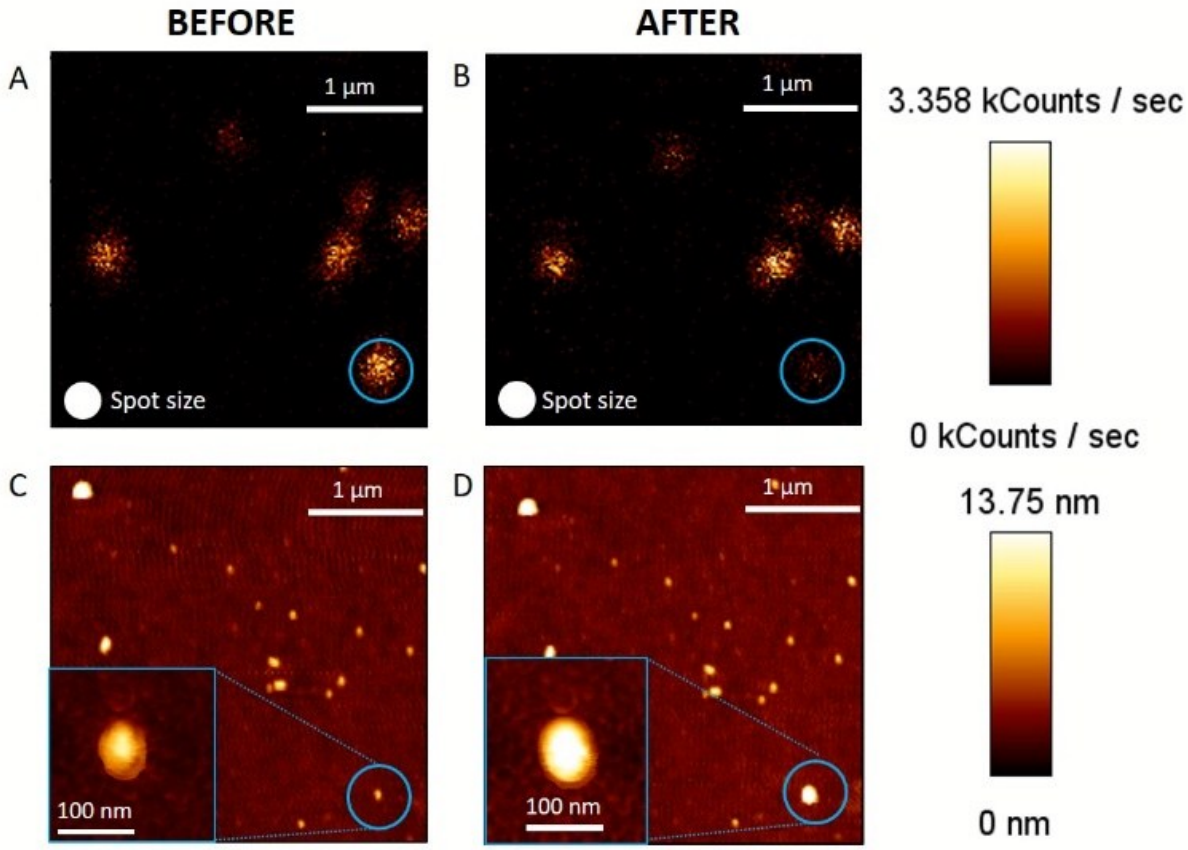

Fig. 2 TPL images ((A) and (B)) of a sample of GNR immobilized onto an ITO coated glass cover slide, before and after the "over-illumination" (F = 125 µJ.cm^{-2}, λ = 800 nm) of the blue circled GNR. Simultaneously acquired AFM topography images ((C) and (D)). The incident polarization, wavelength and power of the excitation laser are the same for both TPL characterization images (A) and (B) (λ = 800 nm; F = 45 µJ.cm^{-2}). High resolution tapping mode AFM scans of the blue circled GNR are displayed as insets of (C) and (D). The complementary SEM image corresponding to the same sample area is available in Fig. S1.

C-1 AFM and SEM characterizations

Smaller scale AFM topographic images of the blue circled GNR were acquired before and after high power resonant laser excitation. They are displayed as insets of Fig. 2C and 2D respectively. AFM topography characterizations show an apparent bigger object after "over-illumination", the rod like shape being preserved. Due to the convolution of the object with the AFM tip, the only directly relevant measurement is the height of the GNR. A 35% increase of the sample height (14 nm before i.e. ~ 10 nm + 4 nm surfactant bilayer and 19 nm after exposure) at the GNR is measured, the GNR appearing globally inflated. Such changes presumably originate either from a change in the GNR itself or a change in the surrounding medium (ITO coating). To get deeper into the topographic characterization and to separate changes from the object from changes in the environment, a complementary SEM analysis was performed (Fig. 3).

As shown in Fig. 3, the SEM image of one "over-illuminated" GNR (in red) presents a distinct halo which appears to be similar in size to the corresponding topography measured in AFM (Fig. 2). Apart from a white SEM contrast revealing a higher conductivity, no measurable morphological change of the GNR itself could be detected, neither in length, nor in diameter. The light halo around the GNR could be attributed to an alteration of the ITO layer which may result from local conductivity variations. Note that the resistivity of ITO decreases upon heating above 375 K.[29]

As displayed in Fig. S2, complementary experiments were performed consisting in very high power illuminations of pristine ITO cover slides (without GNRs). A very high laser illumination was used in order to reach an energy density close to the one expected from local field enhancement effects (between 10 to 100) at resonantly excited GNRs. For F = 50 mJ.cm^{-2}, a change in contrast is observed on the SEM characterization, which appears quite comparable to the one observed around the "over-illuminated" GNRs (halo in Fig. 3). For higher energy densities, local changes of the ITO thickness are evidenced using AFM characterization (see Fig. S2), ranging from local inflation to local hole formation upon further higher exposure as previously reported.[30] Such photo-induced deformation in ITO may explain the apparent height changes observed at "over-illuminated" GNRs using AFM (see Fig. 2).

C-2 Optical characterizations

Since AFM and SEM microscopies do not directly discriminate between a modification of either geometrical or material origins, TPL characterizations were further performed in order

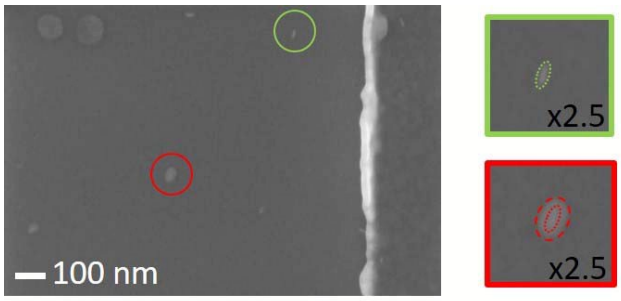

Fig. 3 SEM characterization of single GNRs respectively in the absence (green circled) or consecutively to (red circled) an "over-illumination" of 125 μJ.cm^{-2} with an incident polarization along the longitudinal axis of the GNR and at its longitudinal plasmon resonance wavelength. In the zoomed SEM images on the right, dotted lines delineate the GNR from an additional halo (dashed red lines) regularly observed following an "over-illumination".

to characterize specifically the modified plasmonic properties (longitudinal resonance) of each "over-illuminated" GNRs.

The detailed analysis of the TPL of more than ten single GNRs immobilized onto ITO was systematically carried out, both before and after high power resonant laser illumination (Fig. 4). Considering the origin of TPL,[9] the GNR longitudinal resonance corresponds to the wavelength of maximal TPL intensity. The photo-induced shift in resonance is calculated according to:

$$\Delta\lambda = \lambda^{LR}_{after} - \lambda^{LR}_{before} \qquad (1)$$

where λ^{LR}_{after} and λ^{LR}_{before} are respectively the longitudinal resonance wavelength after and before the "over- illumination" of each considered GNR. λ^{LR}_{before} and λ^{LR}_{after} are derived from TPL excitation spectra, as illustrated in Fig. 4A. Fig. 4A also shows that the TPL intensity maxima before and after an "over-illumination" are quantitatively similar: $I^{TPL}_{before}(\lambda = 800\ nm) \ / \ I^{TPL}_{after}(\lambda = 773\ nm) \approx 1$, i.e. the two-photon luminescence signal can be recovered after a blue-shift of the incident excitation wavelength from 800 nm to 773 nm.

As shown in Fig. 4, a blue-shift of the longitudinal resonance was systematically recorded with a mean shift $\Delta\lambda$ = - 27 nm. The study of the influence of the polarization on the TPL intensity was also performed on the same GNRs before and after the laser exposure. One example of corresponding polar representation is given on Fig. 4C. Whatever the case, either before or after an "over-illumination", the same cos^4(θ) dependence (expected result for GNR in TPL[9]) was observed, where θ is the incident in-plane polarization angle. A maximum of TPL was moreover found for the same incident polarization angle, before and after exposure.

Following a high power laser illumination, the GNRs thus keep their orientation and global rod-like shape but exhibit a blue shift of their longitudinal resonance wavelength. This shift was also revealed by monitoring the TPL emission spectra of the same GNR before and after "over-illumination", as displayed in Fig. S3. The TPL spectra exhibit their characteristic two bands emission,[9] i.e. visible and near infrared bands linked respectively to the transverse and longitudinal resonance wavelengths. Figure S3 shows that over-illumination does not modify the visible band spectrum which keeps centred around 548 nm unlike the IR band which appears clearly shifted to the blue, in direct link with the shift of the longitudinal resonance revealed in figure 4 from the changes in TPL intensity.

Two hypotheses may explain the blue shift of the GNR longitudinal resonance:

(H1) thermally photo-induced morphological changes inducing a decrease of the GNR aspect ratio.[31,32]

(H2) photo-induced modification of the refractive index (n_m) of the surrounding media.

To go one step further and quantify the photo-induced changes, the experimentally determined TPL dependence in wavelength was fitted taking into account that the TPL intensity of small rods varies directly with C_{abs}^2, with C_{abs} the GNR absorption cross section.[9] Considering the quasistatic theory from the Gans-Mie model, the latter can be written:[33]

$$C_{abs} = \frac{2\pi}{3\lambda}\varepsilon_m^{3/2} V \sum_i \frac{\varepsilon_2 / \left(n^{(i)}\right)^2}{\left(\varepsilon_1 + \left[\left(1-n^{(i)}\right)/n^{(i)}\right]\varepsilon_m\right)^2 + \varepsilon_2^2} \qquad (2)$$

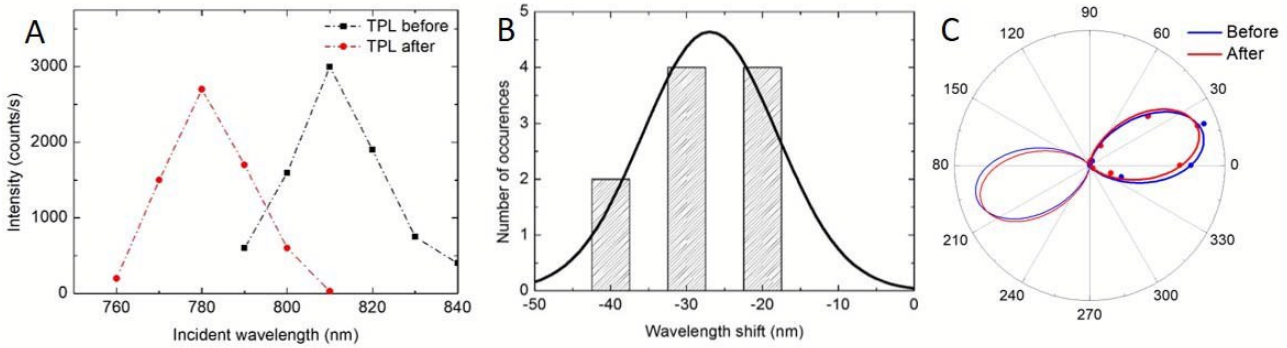

Fig 4 Influence of an "over-illumination" on the TPL luminescence properties of single GNRs (characterization performed using F = 45 μJ.cm^{-2}). (A) TPL excitation spectra recorded for the same single GNR excited along its longitudinal axis before (black squares) and after (red dots) an "over-illumination" (pulse energy density of 125 μJ.cm^2 at resonance). (B) Histogram of the shift of the resonance wavelength of 10 single GNRs following "over-illumination" in comparable conditions. A Gaussian distribution is extrapolated from these data (black line). (C) Polar representation of the TPL intensity of the same single GNR before (blue) and after (red) "over-illumination". Dots corresponds to the experimental data and lines to a cos^4(θ) dependence.

where ε_m is the dielectric constant of the surrounding medium, ε the dielectric constant of the metal with $\varepsilon = \varepsilon_1 + i\varepsilon_2$. λ is the wavelength of the incident light and $n^{(i)}$ the depolarization factors described by:

$$n^{(a)} = \frac{2}{AR^2-1}\left(\frac{AR}{2\sqrt{AR^2-1}}\ln\left(\frac{AR+\sqrt{AR^2-1}}{AR-\sqrt{AR^2-1}}\right) - 1\right) \quad (3)$$

$$n^{(b)} = n^{(c)} = \left(1 - n^{(a)}\right)/2 \quad (4)$$

with *AR* the GNR aspect ratio.

In a first approach, the two hypotheses were separately considered. Namely the 27 nm blue-shift observed for a GNR was either attributed to: a change in aspect ratio *AR* (hypothesis H1), or a change in index of the surrounding medium ε_m (hypothesis H2).

Considering the change in *AR* (hypothesis H1), we show that a blue-shift of 27 nm can be related to an *AR* decrease: $AR_{after} = AR_{before}$ - 0.3 (see Fig. 5). Assuming a constant GNR volume, this means a change from a GNR with 10 nm in diameter and 40 nm in length to a GNR with 10.3 nm in diameter and 38 nm in length. This appears thus as a very small variation, falling under the resolution of our SEM microscope and explaining thus the absence of any apparent change in the GNR geometry upon a high power laser illumination (Fig. 3).

From this, we can calculate the change in absorption cross section for a given wavelength, e.g. the one that was used before high power laser illumination of the GNR, λ = 800 nm. It comes $C_{abs,\ AR=4}$ = 1800 nm² and $C_{abs,\ AR=3.7}$ = 300 nm², i.e. a ratio

$$\left(C_{abs,\ AR=4} \Big/ C_{abs,\ AR=3.7}\right)^2 = 36$$

which is in quite a good agreement with the experimentally observed drop in luminescence following high power illumination

$$I^{before}_{TPL,\ \lambda=800\,nm} \Big/ I^{after}_{TPL,\ \lambda=800\,nm} = 60$$

In a second step, considering a change in ε_m (hypothesis H2), the corresponding refractive index variation is found to be $n_m^{after} = n_m^{before}$ - 0.17, using the same fitting procedure as detailed previously. Such a variation could be assigned to either an ITO alteration or a possible evaporation or degradation of the surfactant. In order to evaluate the validity of such assumptions, high power illumination experiments were performed in the case of GNRs immobilized onto plain glass substrates that are not prone to any photo-induced changes at the overall laser illumination conditions considered here. Here again, the experiment was repeated on around ten GNRs. As for the case of ITO covered glass slides, very similar TPL turn-off effects were observed with the evidence of a similar mean blue-shift of 30 nm (Fig. S4) for the GNR longitudinal resonance before and after "over-illumination". Comparable TPL turn-off effects were also observed with GNR previously deprived of any residual surfactant (UV-ozone treatment following immobilization).

Since comparable results were obtained whatever the considered substrate (ITO coating or glass, presence or absence of any residual CTAB surfactant coating), we can conclude that the main effect of a high power laser excitation of the rods is mostly a change in morphology and more particularly a reduction of the rod aspect ratio of 0.3 (hypothesis H1). Such aspect ratio reduction could reasonably be assigned to gold atom diffusion along the rod,[34] field enhancement processes occurring at the rod tips when excited at their longitudinal resonance.

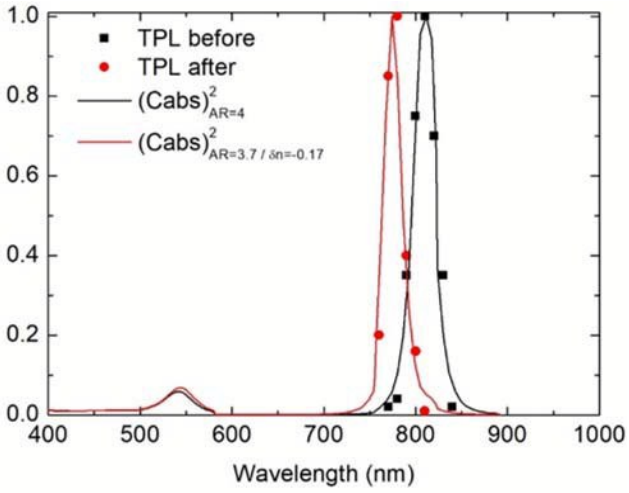

Fig 5 Normalized TPL excitation spectra recorded for the same single GNR excited along its longitudinal axis before (black squares) and after (red dots) an "over-illumination" with a pulse energy density of 125 µJ.cm^{-2} at the GNR longitudinal resonance. The continuous lines are the theoretical adjustment of the experimental data considering the normalized dependence of the GNR absorption cross section C_{abs}^2 as deduced from the Gans-Mie theory for a GNR with an *AR* = 4 (black line) and *AR* = 3.7 or equivalently δn= -0.17 (red line).

C-4 Plasmon induced heating of a GNR illuminated at resonance with 100 µJ.cm^{-2}

Melting energy

According to thermodynamics laws, the energy to melt a gold nanorod can be calculated using the following formula:[35]

$$E = m\left(c_{Au}\Delta T + \Delta H_{fus}\right) \quad (5)$$

where $m = \rho V$ is the mass of the GNR, calculated from its volume *V*, with the bulk Au density[36] ρ of 59 atoms.nm^{-3}, c_{Au} is the specific heat capacity of gold (0.129 J.g^{-1}.K^{-1}), ΔT is the temperature difference between the melting temperature of bulk gold (1337 K) and the room temperature (293 K), and ΔH_{fus} is the fusion enthalpy for gold (63.7 J.g^{-1}). For GNR (Φ = 10 nm, *l* = 40 nm) the melting energy can be estimated to 11 fJ.

Here GNRs were exposed to femtosecond laser excitation. Laser pulse width was shown to have a drastic influence on the heating of nano-objects: femtosecond laser heating is known to be more efficient than nanosecond laser heating as the whole energy from a femtosecond laser pulse can be transferred to the gold nanocrystal before lattice cooling can take place.[26]

Absorbed energy per laser pulse

The absorbed energy E_{abs} by a GNR with an absorption cross section C_{abs} in the case of a laser energy density F is described by:[24]

$$E_{abs} = C_{abs}F \qquad (6)$$

F [mJ.cm^{-2}]	E_{abs} [fJ]	T_{NR} [K]	Emelt [fJ]
0.125	1.4	487	11
2.5	30	T_{fus}	

Table 1 Calculations of the absorbed energy (from equation 6) and the temperature (from equation 7) of a GNR (Φ = 10 nm, l = 40 nm) after one laser pulse for two different energy densities F. The melting energy (derived from equation 5) for such rods is also indicated for comparison

The absorption cross-section of a GNR (Φ = 10 nm, l = 40 nm) was calculated using the Gans-Mie theory. Then the temperature of the GNR following the first pulse is calculated with:[26]

$$T_{NP} = T_0^{NP} + T_0 = \frac{E_{abs}}{mc_{Au}} + T_0 \qquad (7)$$

where T_0 is the initial room temperature (T_0 = 293 K) and E_{abs} the absorbed energy during a single pulse.

As summarized in table 1, the absorbed energy is ten times lower than the Au bulk melting energy in the case of an energy density of 125 µJ.cm^{-2}. The maximum GNR temperature reached after one laser pulse is also lower than the CTAB degradation temperature (533 K),[25] however the temperature reached is presumably high enough to alter the ITO substrate.

To compare with most of the experiments presented in the literature a laser illumination with a much higher energy density of 2.5 mJ.cm^{-2} per pulse was performed. This experiment was realized on several GNRs. Unlike the previous "over-illuminations" carried out at 125 µJ.cm^{-2}, the GNR resonance wavelength after such laser illumination could not be retrieved. A SEM image of one of these GNRs is presented in Fig. 6, evidencing an aspect ratio of AR = 2, i.e. half of the initial one.

The Gans-Mie longitudinal resonance wavelength of a GNR with an aspect ratio of 2 is around 650 nm which is out of the tunability range of our laser source (smallest available wavelength λ = 740 nm). Although high morphological changes could be observed, changes to a sphere were never obtained. As evidenced in table 1 , it thus appears that irradiation with 2.5 mJ.cm^{-2} energy density leads to an absorption around three times higher (30 fJ) than the energy than required for melting (11 fJ), which is a lot more than previously recorded.[23] Here however smaller GNRs were considered (volume reduction of more than 20 compared to Zijlstra et al.[23]), surface effects are to be expected. In particular, for GNRs of reduced size, an exalted cooling is expected[37] as further detailed in the next paragraph

In the above-mentioned experiments, GNRs were exposed during more than one pulse (80 MHz laser repetition rate). The last question is thus to see whether accumulated effects over pulses need to be considered.

Temperature time profile following the first pulse

The applied model to determine the temperature time profile[38] of the GNR after absorption of the first laser pulse was adapted from the case of a spherical nanoparticle.[37] An effective radius r_{eff} is defined using

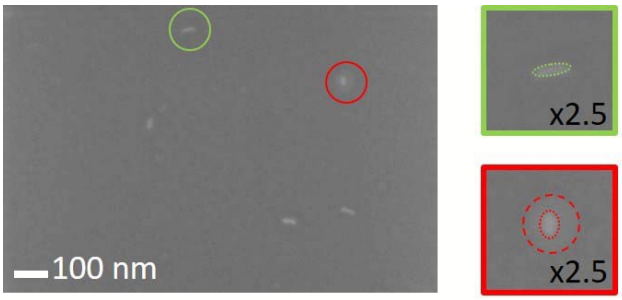

Fig. 6 SEM characterization of single GNRs in the absence (green circle) or after "over-illumination" (red circle). A pulse energy density of 2 5 mJ.cm^{-2} was used with an incident polarization along the longitudinal axis of the GNR and at its longitudinal plasmon resonance wavelength. In the SEM images, dotted lines delineate the GNR from an additional halo observed following high power excitation. The dashed red line delineates a halo around the GNR. The GNR after illumination presents an aspect ratio of around 2. The GNR is clearly shorter than the one illuminated with a 125 µJ.cm^{-2} pulse energy density as shown in Fig. 3.

$$V = \frac{4}{3}\pi r_{eff}^3 \qquad (8)$$

where V is the GNR volume. The absorption of a laser pulse by a metallic NP arises from different processes. Each process is associated with a characteristic time. First, electronic absorption by the gas of free electrons occurs on a time scale of t_P ~ 100 fs.[39] Then the hot electrons thermalize through electron-phonon interactions happening in $t_{elec\text{-}phonon}$ ~1 ps.[40] The characteristic times for the formation of a stationary temperature profile inside the GNR and for heat exchange with the surrounding medium are respectively associated with τ_0 and τ_T which are defined by:[41]

$$\tau_0 \sim \frac{r_{eff}^2}{4\alpha_{Au}} \text{ and } \tau_T \sim \frac{r_{eff}^2}{4\alpha_m} \qquad (9)$$

where α_{Au} is the thermal diffusivity of gold (1.27 x 10^{-4} m^2.s^{-1}) and α_m is the thermal diffusivity of the surrounding media. Here, the GNR were deposited on ITO (α_{ITO} = 1.1 x 10^{-6} m^2.s^{-1}) substrate and the surrounding medium of the GNR is mainly air (α_{air} = 2.2 x 10^{-5} m^2.s^{-1}). Indeed, NRs are in contact with the ITO substrate on only one side facet, which represent less than 1/8 of the GNR surface (considering an octagonal side-facets geometry[27]). We obtain the following mathematical relation:

$$t_p < \tau_0 << \tau_T \sim t_{elec-phonon} << \Delta t \qquad (10)$$

where t_P = 100 fs is the pulse duration, τ_0 = 150 fs, τ_T = 0.9 ps ~ $t_{elec\text{-}phonon}$ and Δt = 12.5 ns the time between two consecutive pulses. During a femtosecond pulse, the absorbed energy is mainly confined in the NP, however due to a fast heat release in the surrounding during the pulse heating, the final temperature rise is much lower than the one expected for a fully decoupled heating process.[37]

The time evolution of the temperature profile was determined throughout two approximations. First the GNR temperature is presumed to be uniform in relation with $k_{Au} >> k_m$ where k_{Au} and k_m are respectively the thermal conductivity of gold (k_{Au} = 314 W.m^{-1}.K^{-1}) and of the surrounding media (k_{air} = 0.03 W.m^{-1}.K^{-1} and k_{ITO} = 4 W.m^{-1}.K^{-1}). The second approximation concerns the initial temperature profile of the GNR which is considered equal to T_{NP} at t = 0. Considering a zero surface resistivity the temperature time profile is described by:[37]

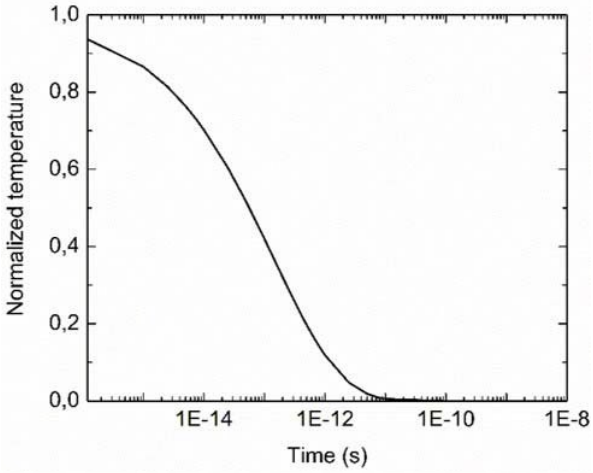

Fig. 7 Evolution of the normalized temperature with time for a nanoparticle with a radius r_{eff} = 8.8 nm considering air as the surrounding medium (semi-log time scale).

$$T_{norm} = \exp\left[-\left(\frac{\alpha_m t}{0.041 r_{eff}^2}\right)^{0.39}\right] \qquad (11)$$

This time dependence is plotted in Fig. 7 considering air as the surrounding media.

For the GNRs (Φ = 10 nm, l = 40 nm) considered, the temperature returns to its initial value within around 10 ps after a pulse absorption. Considering the 80 MHz laser repetition rate, this means that the time period between two pulses Δt = 12.5 ns is more than 1000 times longer. The GNR is fully cooled down to T_0 before the next pulse. No cumulative thermal effect need to be considered and the discussed GNR morphological changes occur within a single laser shot. Considering that these morphological changes lead to a blue-shift of the GNR longitudinal resonance, any longer illumination at the same exciting wavelength results in a decreased absorption, limiting any further photo-induced changes of the GNRs as far as the laser excitation exposure is not too high. Conversely, if the wavelength of the exciting laser excitation is shifted to the blue, in order to match the new GNR longitudinal resonance, additional morphological changes are to be expected. This experiment was performed using reduced cumulative incident energy densities (F = 75 µJ.cm^{-2}) for each illumination. A blue-shift of the GNR resonance wavelength of 5 nm was recorded following each illumination, revealing a continuous morphological variation. Following this line, a precise reshaping of the Au NP can thus be conducted, TPL characterization revealing itself as a highly sensitive tool to follow nanoparticle reshaping.

D. Conclusion

The reversible turn-off of the TPL of small gold nanorods illuminated with rather high energy densities (125 µJ.cm^{-2}) was shown to originate from plasmon-induced reshaping. The energy density considered here for such so-called "over-illumination" are well below the ones previously considered in the literature.[18,20,25,26]. Quite importantly, the objects considered in this work are also very small (Φ = 10 nm, l = 40 nm), thus resulting in characteristic times for heat exchange that happen to be on the same range as the characteristic time for electron-phonon interactions. This is the reason why the final temperature rise in such tiny objects was finally demonstrated to be quite limited, explaining the absence of any melting unlike the case of former studies with particles exhibiting effective radius at least 3 times larger. The GNR plasmon-induced reshaping was investigated in detail at the single object level using complementary analyses ranging from topographic analyses to plasmonic property characterization using TPL. TPL was demonstrated as a highly sensitive technique enabling to detect variation of plasmon resonance smaller than ten nanometers in wavelength. TPL was especially shown to evidence photo-induced morphological changes that happen to be hardly impossible to determine using common imaging methods such as AFM or SEM. From theoretical simulations adapted to GNR, we could show that femtosecond laser illumination with 125 µJ.cm^{-2} energy densities induce a temperature rise around 487 K, high enough to enable gold atom spreading away from the GNR tip but below the melting of the particles. Temperature relaxation was also calculated to be complete between two laser pulses thus avoiding any cumulative effects over many pulses. Importantly, considering a given exciting wavelength (initial GNR longitudinal resonance), the shift of the rod resonance following reshaping leads to reduced absorption which acts as a feedback to stabilize the NP shape and size. Conversely, the continuous matching of the shifted resonance wavelength offers a way to precisely reshape the GNR under illumination, with TPL as a very accurate tool to monitor light-to-heat transfer processes, opening thus new prospects for the controlled photo-induced modification of single plasmonic particles.

Conflicts of interest

There are no conflicts to declare.

Acknowledgements

The authors would like to thank the C'nano 2010 program "INPACT" and ANR Blanc 2012 project "HAPPLE" for financial support of this work. Jeremie BEAL (UTT) is also acknowledged for the realization of landmarks using e-beam lithography.

Notes and references

1 W. L. Barnes, A. Dereux and T. W. Ebbesen, *Nature*, 2003, **424**, 824–830.
2 H. A. Atwater and A. Polman, *Nat. Mater.*, 2010, **9**, 205–213.
3 J. A. Schuller, E. S. Barnard, W. Cai, Y. C. Jun, J. S. White and M. L. Brongersma, *Nat. Mater.*, 2010, **9**, 193.
4 L. Roloff, P. Klemm, I. Gronwald, R. Huber, J. M. Lupton and S. Bange, *Nano Lett.*, 2017, **17**, 7914–7919 and *references therein*.
5 J. Mertens, M.-E. Kleemann, R. Chikkaraddy, P. Narang and J. J. Baumberg, *Nano Lett.*, 2017, **17**, 2568–2574 and *references therein*.
6 V. Amendola, R. Pilot, M. Frasconi, O. M. Maragò and M. A. Iatì, *J. Phys. Condens. Matter*, 2017, **29**, 203002 and *references therein*.
7 G. T. Boyd, Z. H. Yu and Y. R. Shen, *Phys. Rev. B*, 1986, **33**, 7923–7936.
8 N. Gao, Y. Chen, L. Li, Z. Guan, T. Zhao, N. Zhou, P. Yuan, S. Q. Yao and Q.-H. Xu, *J. Phys. Chem. C*, 2014, **118**, 13904–13911.
9 C. Molinaro, Y. El Harfouch, E. Palleau, F. Eloi, S. Marguet, L. Douillard, F. Charra and C. Fiorini-Debuisschert, *J. Phys. Chem. C*, 2016, **120**, 23136–23143.
10 X. Huang, S. Neretina and M. A. El-Sayed, *Adv. Mater.*, 2009, **21**, 4880–4910.
11 Z. Qin and J. C. Bischof, *Chem. Soc. Rev.*, 2012, **41**, 1191–1217.
12 X. Huang, P. K. Jain, I. H. El-Sayed and M. A. El-Sayed, *Lasers Med. Sci.*, 2008, **23**, 217–228.
13 V. K. Pustovalov, A. S. Smetannikov and V. P. Zharov, *Laser Phys. Lett.*, 2008, **5**, 775–792.
14 P. Zijlstra, J. W. M. Chon and M. Gu, *Opt. Express*, 2007, **15**, 12151–12160.
15 Y. Zhang and J. K. Chen, *J. Appl. Phys.*, 2008, **104**, 054910.
16 S. Link, C. Burda, M. B. Mohamed, B. Nikoobakht and M. A. El-Sayed, *J. Phys. Chem. A*, 1999, **103**, 1165–1170.
17 S.-S. Chang, C.-W. Shih, C.-D. Chen, W.-C. Lai and C. R. C. Wang, *Langmuir*, 1998, **15**, 701–709.
18 E. Boulais, R. Lachaine and M. Meunier, *J. Phys. Chem. C*, 2013, **117**, 9386–9396.
19 S. C. Nguyen, Q. Zhang, K. Manthiram, X. Ye, J. P. Lomont, C. B. Harris, H. Weller and A. P. Alivisatos, *ACS Nano*, 2016, **10**, 2144–2151.
20 Y. Li, Z. Jiang, X.-M. Lin, H. Wen, D. A. Walko, S. A. Deshmukh, R. Subbaraman, S. K. R. S. Sankaranarayanan, S. K. Gray and P. Ho, *Sci. Rep.*, 2015, **5**, 8146.
21 A. Plech, S. Ibrahimkutty, S. Reich and G. Newby, *Nanoscale*, 2017, **9**, 17284–17292.
22 G. González-Rubio, P. Díaz-Núñez, A. Rivera, A. Prada, G. Tardajos, J. González-Izquierdo, L. Bañares, P. Llombart, L. G. Macdowell, M. Alcolea Palafox, L. M. Liz-Marzán, O. Peña-Rodríguez and A. Guerrero-Martínez, *Science*, 2017, **358**, 640.
23 P. Zijlstra, J. W. M. Chon and M. Gu, *Phys. Chem. Chem. Phys.*, 2009, **11**, 5915–5921.
24 W. Albrecht, T.-S. Deng, B. Goris, M. A. van Huis, S. Bals and A. van Blaaderen, *Nano Lett.*, 2016, **16**, 1818–1825.
25 M. Gordel, J. Olesiak-Banska, K. Matczyszyn, C. Nogues, M. Buckle and M. Samoc, *Phys. Chem. Chem. Phys.*, 2014, **16**, 71–78.
26 S. Link, C. Burda, B. Nikoobakht and M. A. El-Sayed, *J. Phys. Chem. B*, 2000, **104**, 6152–6163.
27 J. Xiao and L. Qi, *Nanoscale*, 2011, **3**, 1383–1396.
28 T. K. Sau and C. J. Murphy, *Langmuir*, 2004, **20**, 6414–6420.
29 V. S. Reddy, K. Das, A. Dhar and S. K. Ray, *Semicond. Sci. Technol.*, 2006, **21**, 1747.
30 N. N. Nedyalkov, P. A. Atanasov and M. Obara, *Nanotechnology*, 2007, **18**, 305703.
31 Y. Liu, E. N. Mills and R. J. Composto, *J. Mater. Chem.*, 2009, **19**, 2704–2709.
32 H. Petrova, J. P. Juste, I. Pastoriza-Santos, G. V. Hartland, L. M. Liz-Marzan and P. Mulvaney, *Phys. Chem. Chem. Phys.*, 2006, **8**, 814–821.
33 R. Gans, *Ann. Phys.*, 1915, **47**, 270–284.
34 S. Inasawa, M. Sugiyama and Y. Yamaguchi, *J. Phys. Chem. B*, 2005, **109**, 3104–3111.
35 S. Link and M. A. El-Sayed, *J. Chem. Phys.*, 2001, **114**, 2362–2368.
36 M. M. Alvarez, J. T. Khoury, T. G. Schaaff, M. N. Shafigullin, I. Vezmar and R. L. Whetten, *J. Phys. Chem. B*, 1997, **101**, 3706–3712.
37 G. Baffou and H. Rigneault, *Phys. Rev. B*, 2011, **84**, 035415.
38 V. K. Pustovalov, *Laser Phys. Lett.*, 2005, **2**, 401–406.
39 H. Inouye, K. Tanaka, I. Tanahashi and K. Hirao, *Phys. Rev. B*, 1998, **57**, 11334–11340.
40 J. Hodak, I. Martini and G. V. Hartland, *Chem. Phys. Lett.*, 1998, **284**, 135–141.
41 V. K. Pustovalov, *Chem. Phys.*, 2005, **308**, 103–108.